Lean-Burn Stationary Natural Gas Engine Operation With a Prototype Laser Spark Plug

Dustin L. McIntyre
Steven D. Woodruff
John S. Ontko

National Energy Technology Laboratory,
United States Department of Energy,
3610 Collins Ferry Road,
Morgantown, WV 26507

An end pumped passively Q-switched laser igniter was developed to meet the ignition system needs of large bore lean burn stationary natural gas engines. The laser spark plug used an optical fiber coupled diode pump source to axially pump a passively Q-switched Nd:YAG laser and transmit the laser pulse through a custom designed lens. The optical fiber coupled pump source permits the excitation energy to be transmitted to the spark plug at relatively low optical power, less than 250 W. The Q-switched laser then generates as much as 8 mJ of light in 2.5 ns, which is focused through an asymmetric biconvex lens to create a laser spark from a focused intensity of approximately 225 GW/cm^2. A single cylinder engine fueled with either natural gas only or hydrogen augmented natural gas was operated with the laser spark plug for approximately 10 h in tests spanning 4 days. The tests were conducted with fixed engine speed, fixed boost pressure, no exhaust gas recirculation, and laser spark timing advance set at maximum brake torque timing. Engine operational and emissions data were collected and analyzed.
[DOI: 10.1115/1.4000292]

1 Introduction

With increasing restrictions being placed on reciprocating engine emissions and increasing demands for energy efficiency, the traditional spark ignition system is reaching its practical limit of durability, and effectiveness in igniting ultralean fuel/air mixtures of natural gas. Laser ignition has the potential to advance large bore lean burn natural gas fueled engine technology by improving ignition system durability and ignitability, and has shown the possibility of improved efficiency and lower emissions [1–13]. Although laser ignition shows promise as a durable high-energy ignition system for future high efficiency internal combustion engines, it has suffered from issues such as large size, high cost, and low efficiency. The development of a miniaturized low cost laser ignition system would enable advancement in the development and commercialization of higher efficiency lower emission engines. This and prior laser spark plug development work [14–16] was intended to improve the overall cost and efficiency of the laser ignition system.

The present study focuses on the ignition and operation of a single cylinder research engine with a newly developed laser diode end pumped, passively *Q*-switched laser. The design parameters and operational techniques of the miniaturized laser system were drawn from prior research [14–16]. The advantages of laser spark ignition for natural gas fueled engines has been demonstrated with open-air optical coupling [1–12] and capillary optical coupling [13]. The engines run smoother and at leaner mixtures with laser ignition when compared with electrical spark ignition [1–4]. What remains to be demonstrated is a cost effective, durable, and safe laser spark plug ignition system, which can be installed or retrofitted to any natural gas fueled engine currently using electrical spark plug ignition. The fiber optic coupled end pumped laser sparkplug is a significant advance toward producing such a commercial laser spark plug system. The fiber optic distribution of pumping energy to a number of laser spark plugs will allow for the centralization and sharing of expensive diode laser pumps away from the heat and vibration of the engine.

Contributed by the IC Engine Division of ASME for publication in the JOURNAL OF ENGINEERING FOR GAS TURBINES AND POWER. Manuscript received May 21, 2009; final manuscript received May 22, 2009; published online April 19, 2010. Editor: Dilip R. Ballal.

Previous engine studies at the National Energy Technology Laboratory (NETL) have focused on the development of experimental data to support laser ignition of lean natural gas mixtures as a viable method of improving efficiency, reducing emissions, and extending the lean limit of operation [1–4,16]. The engine studies were performed with laboratory scale flash lamp pumped actively *Q*-switched neodymium doped yttrium aluminum garnet (Nd:YAG) lasers [1–4]. More recent engine studies were performed to verify design parameters for a miniaturized diode side pumped passively *Q*-switched laser developed at NETL [16]. The current work focuses on the extension of the side pumped laser work to the development of an end pumped laser system with greatly improved operational parameters. The newly developed end pumped laser was packaged in such a manner that it was relatively insensitive to heat and vibration, which allowed it to be directly attached to the engine unlike the previous side pumped laser design.

2 Laser Spark Plug Design

The end pumped laser design was based on earlier studies of a prototype side pumped passively *Q*-switched laser spark plug [14–16]. The end pumped laser has significant advantages over conventional side pumped lasers. The most distinct advantage is the considerable increase in beam overlap efficiency as compared to the side pumped laser. The beam overlap is defined as the coincidence between the highly pumped or excited portion of the laser crystal, where the most optical storage occurs, and the cross section of the laser crystal that interacts with the feedback cavity to produce useful laser output. The laser action boundary encompasses this active cross section of the laser medium. The less efficient excitation and laser action boundary overlap of the side pumped system is shown in Figs. 1 and 2.

The high absorption of the pump energy by the laser crystal causes the highly excited areas to be concentrated near the edge of the laser rod. This concentration of excited states induces noncylindrically symmetric thermal lensing, which results in a significant loss in the laser system. The thermal lensing is due to the heating and subsequent expansion of the crystalline material. The expansion of the crystal matrix results in a minor change in the material density. This minor change in density induces internal stresses within the crystal lattice producing off-axis refractive in-

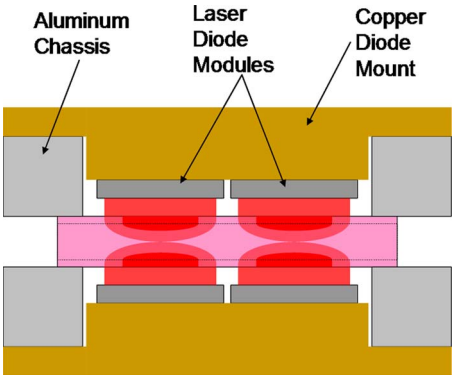

Fig. 1 Lateral view of diode side pumped laser showing absorption patterns

dex gradients giving rise to the crystals distorted lens like behavior. The concentration of the excited states near the edge of the rod leads to poor overlap between the areas of high optical storage and the areas within the laser action boundary that produce useful intracavity flux and subsequent high-energy laser output. This poor overlap significantly reduces the potential output of the system. The improved overlap between the excited areas and the laser action boundary produced by the end pumped geometry are shown in Figs. 3 and 4.

With the pump beam symmetric on the lasing axis, the thermal effects are symmetric as well. The implication here is that while there will be some thermal lensing, it will exhibit less distortion and cavity symmetry is maintained. So while cooling of the laser rod will still be necessary, the thermal effects will be less important and less cooling will be required. It should also be noted that passive Q-switching is significantly easier with the end pumped laser, giving more flexibility to attaining high peak powers and shorter pulse widths, as compared to the previous work with the side pumped laser system.

The Nd:YAG laser rod was 10 mm long $\times$ 5 mm diameter, polished flat, and antireflection coated on both ends. The rod was mounted in a 10 mm long $\times$ 25 mm diameter aluminum block

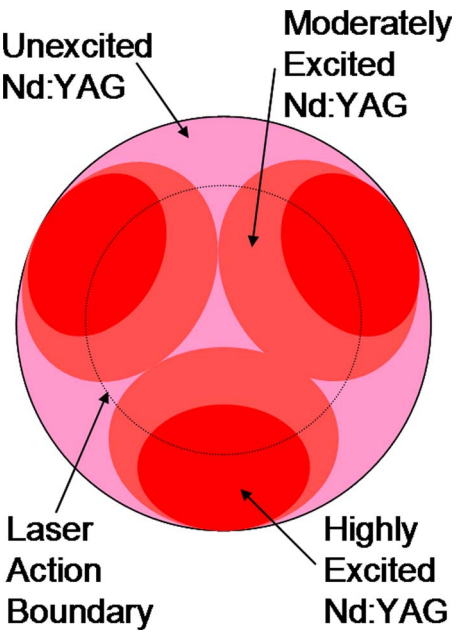

Fig. 2 Cross section of side pumped laser rod showing off-centered and uneven absorption pattern

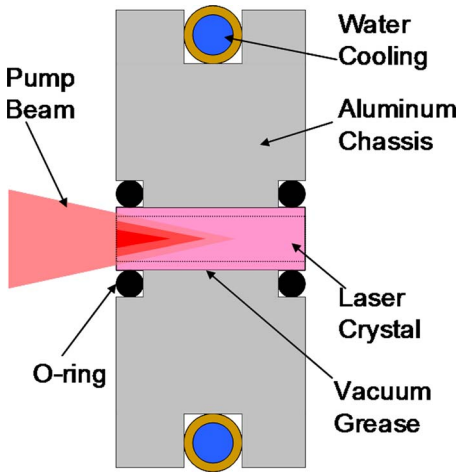

Fig. 3 Lateral view of diode end pumped laser showing absorption patterns

with a single turn of copper tubing around the outside to cool the block with water flow (Refer to Fig. 3). The center of the block was bored to 5 mm diameter and the ends counter bored to accommodate o-rings sized to friction fix the rod in place. Silicone vacuum grease was used to provide thermal contact of the Nd:YAG rod to the aluminum mounting block. Figure 5 shows the end pumped laser cavity construction and optical components.

The laser cavity was defined by mounting the components in a pair of side adjusting flexure mounts, which provided optical fixtures on both sides such that the laser rod and the Cr:YAG passive Q-switch could be mounted on the fixed inside positions, and the mirrors to the adjustable outside positions. In this way the optical cavity was $\sim$32 mm in length. The Cr:YAG crystal was 5 mm square and mounted in a 1 in. diameter mount. The rear reflector was a 99.5% reflectivity mirror at 1.06 μm and 95% transmission at 810 nm. The output coupler was a 30% reflectivity mirror at

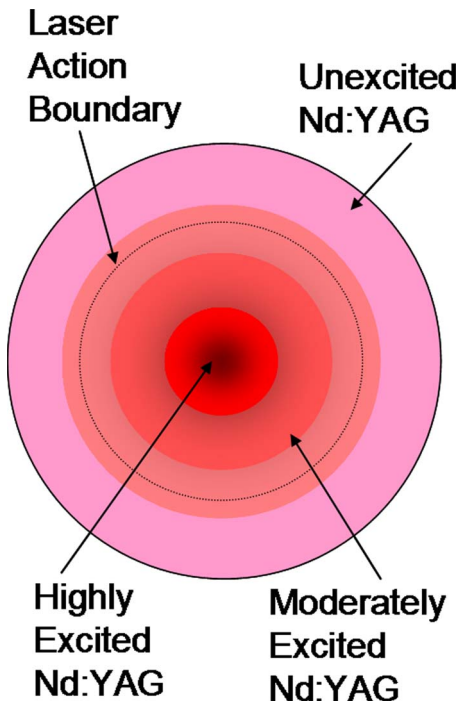

Fig. 4 Cross section of end pumped laser rod showing centered and even absorption pattern

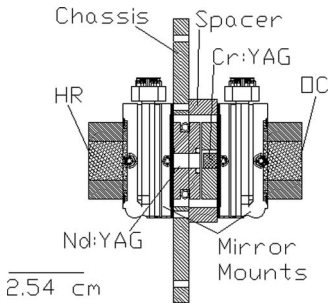

Fig. 5 End pumped laser cavity construction and optical components

1.06 μm. The laser cavity was mounted on a custom machined aluminum chassis. The optical pumping configuration used a 20 mm focal length aspherical collimating lens and a 40 mm focal length focusing lens to relay the pump light from the optical fiber to the Nd:YAG rod. The end pumped laser schematic is shown in Fig. 5, where it is compared to the prior side pumped laser design. The pump light was delivered through a 600-μm optical fiber with a sub miniature A (SMA) (fiber optic connector type) termination. The fiber coupled pump laser was rated at >400 W at 810 nm and cooled with a recirculating water bath set at 27°C. When operated on the engine, the laser system controller was triggered by the engine control system with a transistor–transistor logic (TTL) pulse. Figure 6 shows a scale comparison of the current end pumped laser design and the previous side pumped laser design.

Delivery of the optical pumping energy through an optical fiber provides a near point source, which can be shaped through simple lenses to provide a small diameter cylinder of pump excitation co-axial with the lasing axis through the rear laser reflector. Another advantage is that the pump excitation is less than 250 W and easily transmitted through an optical fiber. This is easily accomplished compared to attempting to transmit a laser pulse in excess of 3 MW in ~5 ns pulses through a near single mode optical fiber in order to retain the high mode quality required to focus and generate a laser spark. The pumping energy was transmitted in 0.5 μs pulses, which was easily handled with the available optics and allowed for a greatly simplified optical distribution system. Jitter of the delivered Q-switched pulse from the control TTL trigger was on the order of 4 μs.

Table 1 lists the input and output parameters for the side pumped and end pumped laser systems as a brief comparison. Table 1 shows that the current end pumped laser design is approximately four times shorter than the previous side pumped design, which leads to a reduced output pulse width and increased output peak power. The current end pumped laser design requires approximately four times less input pump power than the previous side pumped design greatly increasing the overall efficiency of the system.

Table 1 Prototype laser parameter comparison

	Side pumped	End pumped
OC (%)	30	30
QSW (%)	32	20
Nd (%)	0.5	0.9
P_{pump} (W)	1007	240
L_{cavity} (cm)	13.15	3.20
E_o (mJ)	23	8
t_p (ns)	10	2.5
P_{peak} (MW)	2.3	3.2
M^2	6.55	5.5
D_{beam} (mm)	~3	~2.5
Lens f_L (mm)	31	14.37
I (GW/cm^2)	~35	~225
Engine speed (rpm)	600	1800

To steer the laser beam to the spark plug focusing lens, a pair of 2 deg, antireflection coated, wedge prisms was mounted in rotating mounts and positioned immediately after the output coupling mirror. The assembly was mounted to the head of the engine with a custom machined mount and positioned such that the laser was centered on the spark plug lens tube. Figure 7 shows a structural diagram of the laser spark plug associated optics and the engine adaptor.

Previous engine studies have utilized sapphire lenses to focus the laser beam and provide the required high-pressure seal to the combustion chamber [1–4,14,16]. Sapphire was preferred because it can be brazed directly to the metal spark plug body. This sealing technique made for a very robust design although it was very expensive. In addition, the sapphire lenses are typically available only as planoconvex singlets and custom lens designs in sapphire significantly add to the cost of the already costly sealing mechanism. The current design uses a fused silica lens with an asymmetric biconvex design and a silicone rubber seal. Fused silica was selected because it is more easily ground into custom shapes and can easily withstand high temperature environments. The lens was designed with a sufficient thickness to handle the pressure, and two distinct curvatures similar to best form lenses used to focus lasers to the diffraction limit. This design does not focus to

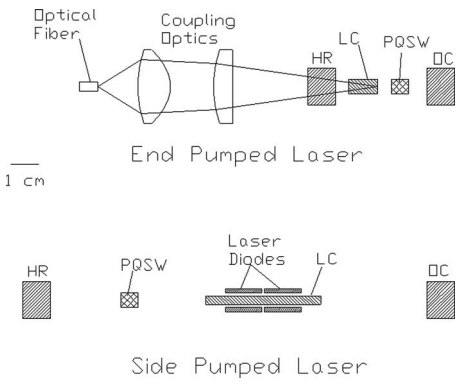

Fig. 6 Scale comparison of end pumped laser from current work and side pumped laser from previous work

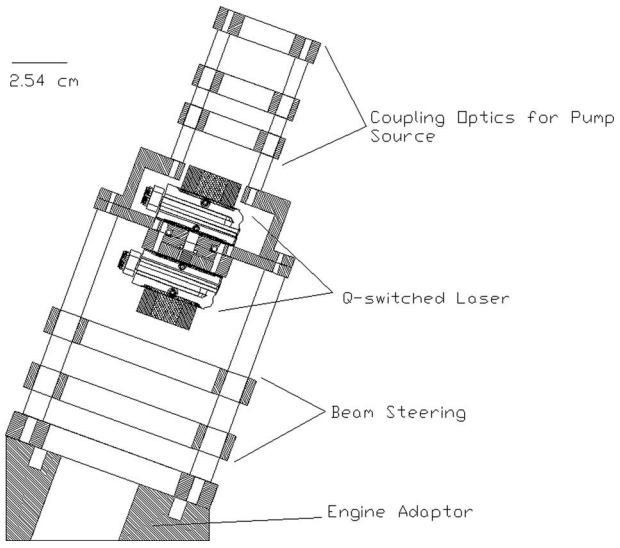

Fig. 7 Structural diagram of laser spark plug, associated optics and engine adaptor

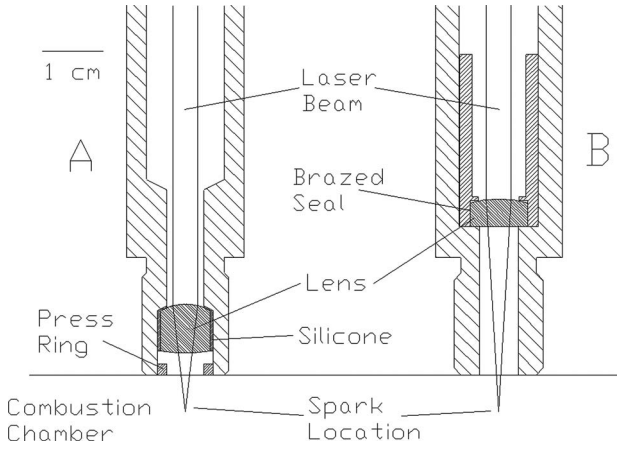

Fig. 8 Sealing lens design comparison: (*a*) current design and (*b*) previous design

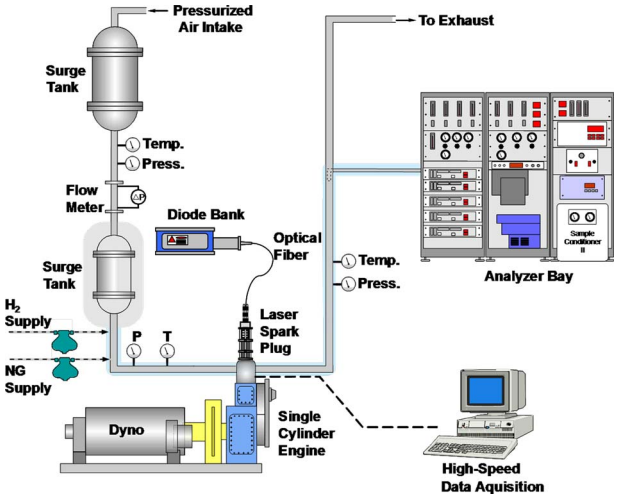

Fig. 10 Engine test facility schematic

the diffraction limit, but does focus the laser beam to an approximately ten times smaller beam waist than a planoconvex singlet of similar focal length. The deep wall thickness also enabled the window to be sealed into the spark plug body with a high temperature silicone rubber, significantly reducing cost and complexity in the spark plug design. Lifetime tests on this sealing mechanism need to be performed, but there was no deterioration during the present tests. Figure 8 shows the sealing lens design differences for the current and previous experiments.

The sparkplug lens insert was configured to be a direct replacement of an aircraft style, extended barrel, side-gap type spark plug or equivalent. The body was machined of stainless steel and terminated with 0.75 in. (19.05 mm) of 18 mm thread. A 6 mm hole was bored through the threaded end and counter sunk with a 9 mm diameter by 10 mm opening to accept the fused silica lens. The lens and the counter sunk hole were primed with room temperature vulcanizing (RTV) primer and allowed to dry 30 min before installation into the spark plug assembly. The silicone sealant was applied and allowed to cure 24 h, and then heat cured up to 250°C over an 8 h period per the RTV product sheet. After cleaning excess material from the face of the lens, a stainless steel ring was press fit to the pressure side of the lens. The ring did not make contact with the lens and was only present as a safeguard to prevent the lens from falling into the combustion chamber should the sealant fail. Figure 9 shows a photo of the end pumped laser spark plug engine setup.

3 Engine Test Cell and Experimental Setup

The test cell used for experimentation in this work is located at the U.S. Department of Energy's National Energy Technology Laboratory facility in Morgantown, WV. The test cell consists of a Ricardo Proteus single cylinder research engine, dynamometer, and control and instrumentation hardware for measuring and/or modifying many of the operational aspects of the engine [17].

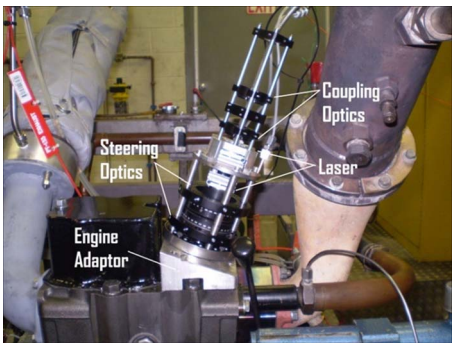

Fig. 9 Photo of laser spark plug engine setup

The cell is outfitted with a 75 kW dynamometer, which was used to motor the engine for starting before fuel or spark energy was introduced. The dynamometer was used to regulate the operational speed of the engine under fueled conditions. The cell includes fuel flow monitors for natural gas and hydrogen and is equipped with temperature controls for the engine coolant, oil, intake air, and the test cell. These controls are vital to the consistency of any tests that are spread over the course of days, weeks, or months because they allow for the most similar test situations independent of daily or operational differences. Figure 10 shows a basic schematic of the engine test cell.

The engine was instrumented with high and low speed data acquisition systems, which recorded all major engine parameters. A gas sample train allowed the measurement of O_2, total hydrocarbons, CO_2, CO, and NO_x concentrations in the exhaust. Ignition timing in spark ignition (SI) operation was computer controlled and variable over a wide range. Currently, the engine may be fueled by natural gas or hydrogen or any mixture of the two. It was desirable to compare the current data set to the laser ignition and electrical spark ignition data taken previously at NETL; unfortunately, the single cylinder engine had undergone a complete rebuild making the previous data incomparable due to minor changes in the engine setup. Also the two CO analyzers were not in working order for the experiment and the tests were not able to be repeated due to budgetary constraints.

The goal of the engine testing was to study how the engine responded when ignited by the test laser with the multiple fuel compositions. For the present work, two fuels were used: (1) natural gas and (2) a mixture of natural gas (80% by volume) and hydrogen (20% by volume). The tests spanned three equivalence ratios, $\varphi=0.7$, $\varphi=0.8$, and $\varphi=0.9$, and were run at fixed boost pressure (20 kPa gauge) and speed (1800 rpm) with maximum brake torque timing at each φ. Timing was adjusted as shown in Table 2 to approximate maximum brake torque timing. Three complete randomized test replicates were run with natural gas and

Table 2 Laser ignition spark timing

φ	Natural gas (btdc)	NG+H_2 (btdc)
0.9	20.0	10.0
0.8	22.6	12.6
0.7	30.0	18.0

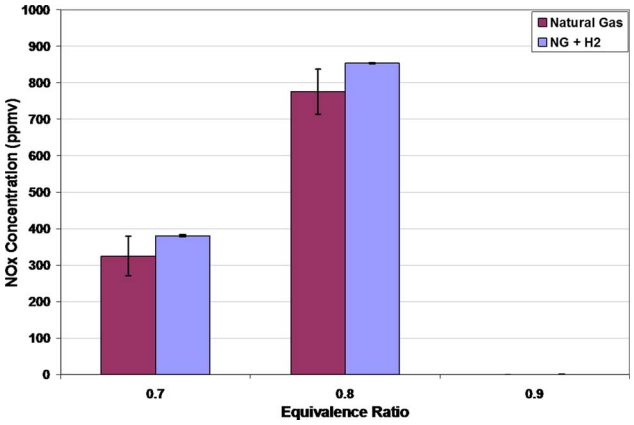

Fig. 11 Total NO_x emissions data for the two tests as a function of equivalence ratio

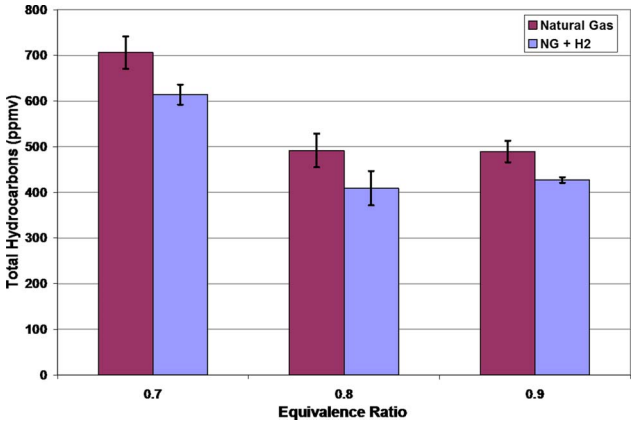

Fig. 13 Total hydrocarbons emissions data for the two tests as a function of equivalence ratio

two with the H_2 mixture. Time and budgetary constraints prevented a third test replicate for the hydrogen blend testing. The experiments were run blockwise by fuel composition and the levels of φ were randomized within each block.

4 Emission Data

Engine emissions data were taken to determine the differences between the exhaust emissions concentrations due to the operation of the engine with the different fuels. Figures 11–13 show the measured NO_x, CO_2, and total hydrocarbon (THC) emissions with respect to equivalence ratio. The concentrations were corrected to 15% O_2. The data error bars depict a single standard deviation. Figure 11 illustrates the NO_x emissions for both fueling conditions at each respective equivalence ratio. The data show a significant increase in the NO_x emissions as the equivalence ratio is increased. NO_x production is highly temperature dependent and as the equivalence ratio is raised the combustion temperature increases, and therefore the NO_x production is significantly increased. An analysis of variance of the NO_x data was performed to determine the effect that both the fuel and the equivalence ratio had on the data. The equivalence ratio was found to have a significant effect on the NO_x concentration, which was expected. The effect of the fuel hovered around detectability (if the criterion for statistical significance is taken to be a probability of 0.05), but the NO_x concentration increased sharply with increasing φ. Unfortunately, the NO_x analyzer was saturated at $\varphi=0.9$, so these points were omitted from the analysis.

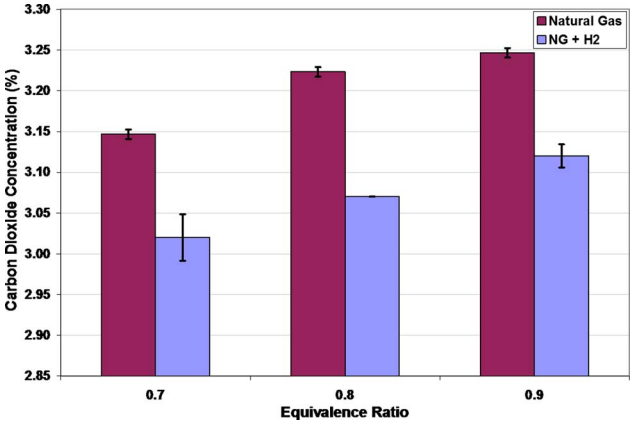

Fig. 12 Carbon dioxide emissions data for the two tests as a function of equivalence ratio

Figure 12 shows that the CO_2 emissions increased as a function of the equivalence ratio for both fuel types. The introduction of the hydrogen into the fuel produced a decrease in CO_2 concentration primarily because of the overall decrease in hydrocarbons in the fuel. The combustion of hydrogen does not produce CO_2 as a byproduct. The increase in the CO_2 concentration as a function of the equivalence ratio is an indication of completeness of combustion. As the fuel mixture is leaned out the CO_2 concentration decreases in conjunction with a complementary increase in total hydrocarbons in the exhaust stream, which can be seen in Fig. 13. The analysis of variance performed on the CO_2 data determined that both the fuel and the equivalence ratio had a significant affect on the CO_2 concentrations.

Figure 13 shows that the total hydrocarbon concentration in the exhaust stream decreases as an increasing function of the equivalence ratio. This is an indication that as the equivalence ratio approaches stoichiometric the combustion process is becoming more and more complete. This was consistent with both Figs. 11 and 12 previously. The THC concentration also decreases slightly with the addition of hydrogen to the fuel due to the displacement of the hydrocarbons by the hydrogen.

5 Conclusions

The present study focused on the ignition and operation of a single cylinder research engine with a newly developed diode end pumped passively Q-switched laser spark plug. The design, construction, and operational techniques of the miniaturized laser system were drawn from prior research. The advantages of laser spark ignition for natural gas fueled engines have been demonstrated previously at NETL. The end pumped test laser was constructed with a 30% flat output coupler with a flat high reflector, 20% Q-switch initial transmission, and a 0.9% Nd concentration rod all pumped by 240 W of optical power.

- The test laser output pulse energy was approximately 8 mJ, with a pulsewidth of 2.5 ns, and an M^2 value of 5.5, which produced a focal intensity of approximately 225 GW/cm^2.
- The end pumped laser spark plug was mounted directly to the engine and was operated at 1800 rpm (previous side pumped laser spark plug engine work was kept under 600 rpm and the laser was mounted on an isolated bench to reduce the effects of temperature and vibration).

Engine emission data were taken to determine the differences between the exhaust emission concentrations due to the operation of the engine with the different fuels, natural gas, and natural gas blended with hydrogen. The engine emissions, when operated with natural gas alone, were typical considering the operating parameters and were as follows.

- The NO_x concentration increased with increasing equivalence ratio due to increasing combustion temperatures.
- CO_2 concentration increased with increasing equivalence ratio due to more complete ignition and combustion.
- The total hydrocarbons decreased with increasing equivalence ratio, which was due to more complete ignition and combustion.

The addition of 20% hydrogen (by volume) to the natural gas produced results that were expected and are as follows.

- The NO_x concentrations increased with increasing equivalence ratio due to the higher combustion temperatures that were produced by the addition of the higher energy fuel.
- The CO_2 concentrations were reduced across all of the equivalence ratio values because the addition of hydrogen dilutes the overall availability of carbon in the fuel mix.
- The total hydrocarbons decreased because the methane was more completely burned and the unburned hydrogen does not add to the concentration of unburned hydrocarbons.

The engine performed as well with laser ignition as with spark ignition with the addition of smoother operation and an extended lean limit with both natural gas and hydrogen augmented natural gas. Past work has focused on the development of a stand alone laser spark plug whereas future work will focus on the distribution of optical pumping energy to laser spark plugs at multiple cylinders.

Acknowledgement

The authors would like to thank the National Energy Technology Laboratory (NETL), U.S. Department of Energy. They would also like to thank the reciprocating engine program contract support personnel, Doug Horton and Todd Worstell, and West Virginia University Mechanical and Aerospace Engineering graduate students, Sam George and Jacinto Solano.

References

[1] McMillian, M. H., Richardson, S., Woodruff, S. D., and McIntyre, D., 2004, "Laser-Spark Ignition Testing in a Natural Gas-Fueled Single-Cylinder Engine," SAE Paper No. 2004-01-0980.
[2] Richardson, S., McMillian, M. H., Woodruff, S. D., and McIntyre, D. L., 2004, "Misfire, Knock and NOx Mapping of a Laser Spark Ignited Single Cylinder Lean Burn Natural Gas Engine," SAE Paper No. 2004-01-1853.
[3] McMillian, M. H., Woodruff, S. D., Richardson, S. W., and McIntyre, D. L., 2004, "Laser Spark Ignition: Laser Development and Engine Testing," ASME Paper No. ICEF2004-917.
[4] Richardson, S. W., McMillian, M. H., Woodruff, S. D., Worstell, T., and McIntyre, D. L., 2006, "Laser Spark Ignition of a Blended Hydrogen-Natural Gas Fueled Single Cylinder Engine," ASME Paper No. ICES2006-1397.
[5] Ivanic, Z., Ayala, F., Goldwitz, J. A., and Heywood, J. B., 2005, "Effects of Hydrogen Enhancement on Efficiency and NOx Emissions of Lean and EGR-Diluted Mixtures in a SI Engine," SAE Paper No. 2005-01-0253.
[6] Aherns, D. L., Yalin, A. P., Olsen, D. B., and Kim, G. H., 2005, "Development of an Open Path Laser Ignition System for a Large Bore Natural Gas Engine: Part 1 System Design," ASME Paper No. ICEF2005-1060.
[7] Dale, J. D., Smy, P. R., and Clements, R. M., 1978, "Laser Ignited Internal Combustion Engine—An Experimental Study," SAE Paper No. 780329.
[8] Alger, T., Mehta, D., Chadwell, C., and Roberts, C., 2005, "Laser Ignition in a Pre-Mixed Engine: The Effect of Focal Volume and Energy Density on Stability and the Lean Operating Limit," SAE Paper No. 2005-01-3752.
[9] Bihari, B., Gupta, S. B., Sekar, R. R., Gingrich, J., and Smith, J., 2005, "Development of Advanced Laser Ignition System for Stationary Natural Gas Reciprocating Engines," ASME Paper No. ICEF2005-1325.
[10] Kopecek, H., Charareh, S., Lackner, M., Forsich, C., Winter, F., Klausner, J., Herdin, G., Weinrotter, M., and Wintner, E., 2005, "Laser Ignition of Methane-Air Mixtures at High Pressures and Diagnostics," ASME J. Eng. Gas Turbines Power, **127**, pp. 213–219.
[11] Herdin, G., Klausner, J., Wintner, E., Weinrotter, M., and Graf, J., 2005, "Laser Ignition a New Concept to Use and Increase the Potentials of the Gas Engines," ASME, Paper No. ICEF2005-1352.
[12] Smith, J. R., 1979 "Comparison of Ignition Locations in a High Swirl Engine," Sandia Laboratories Report No. SAND-79-8715.
[13] Ahrens, D. L., Olsen, D. B., and Yalin, A. P., 2005, "Development of an Open Path Laser Ignition System for a Large Bore Natural Gas Engine: Part 2 Single Cylinder Demonstration," ASME Paper No. ICES2005-1317.
[14] McIntyre, D. L., 2007, "A Laser Spark Plug Ignition System for a Stationary Lean-Burn Natural Gas Reciprocating Engine," Ph.D. thesis, West Virginia University, Morgantown, WV.
[15] McIntyre, D. L., Woodruff, S. D., McMillian, M. H., Richardson, S. W., and Gautam, M., 2007, "Laser Spark Plug Development," SAE Paper No. 2007-01-1600.
[16] McIntyre, D. L., Woodruff, S. D., McMillian, M. H., Richardson, S. W., and Gautam, M., 2008, "Lean-Burn Stationary Natural Gas Reciprocating Engine Operation With a Prototype Miniature Diode Side Pumped Passively Q-Switched Laser Spark Plug," ASME Paper No. ICES2008-1696.
[17] 1986, Proteus Single Cylinder Research Engine No. 102 Instruction and Operating Manual.